Inorganic Chemistry

ARTICLE

pubs.acs.org/IC

Porous $ZnCo_2O_4$ Nanowires Synthesis via Sacrificial Templates: High-Performance Anode Materials of Li-Ion Batteries

Ning Du, Yanfang Xu, Hui Zhang, Jingxue Yu, Chuanxin Zhai, and Deren Yang*

ABSTRACT: A simple microemulsion-based method has been developed to synthesize $ZnCo_2(C_2O_4)_3$ nanowires that can be transformed to porous $ZnCo_2O_4$ nanowires under annealing conditions. The morphology of porous $ZnCo_2O_4$ nanowires can be tuned by the initial $ZnCo_2(C_2O_4)_3$ nanowires and the annealing temperatures. The as-synthesized porous $ZnCo_2O_4$ nanowires have been applied as anode materials of Li-ion batteries, which show superior capacity and cycling performance. The porous one-dimensional (1D) nanostructures and large surface area are responsible for the superior performance. Moreover, it is indicated that porous $ZnCo_2O_4$ nanowires synthesized at low annealing temperature (500 °C) show larger capacity and better cycling performance than that prepared at high annealing temperature (700 °C), because of their higher porosity and larger surface area.

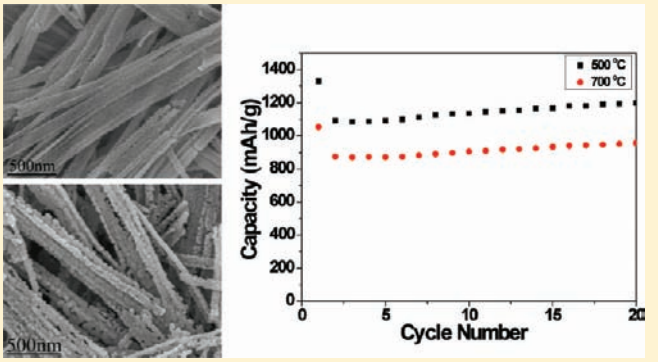

INTRODUCTION

Since the discovery of 3d transition-metal oxides with good performance as the rechargeable anode of Li-ion battery, a worldwide effort has been made to improve their capacity, cycling performance, and initial columbic efficiency.[1] Among the 3d transition-metal oxides, cobalt oxides (Co_3O_4, CoO) have shown the highest capacity and best cycling performance, compared to nickel oxide and iron oxides.[2−5] However, many efforts are made to replace Co_3O_4 partially by environment-friendly and less-expensive alternative metals to lower the toxicity and reduce the cost, to some extent.[6−9] As a result, the ternary cobalt-based metal oxides such as $ZnCo_2O_4$ have been realized as anode materials of Li-ion batteries.[10,11] For example, Sharma et al. synthesized $ZnCo_2O_4$ nanoparticles with diameters of ∼15−20 nm by a low-temperature and cost-effective urea combustion method. Galvanostatic cycling of $ZnCo_2O_4$ nanoparticles in the voltage range of 0.005−3.0 V versus Li at 60 mA g^{-1} gave reversible capacities of 900 mA h g^{-1}, which is even larger than the Co_3O_4 nanoparticles.[11]

In the research of Li-ion batteries, recent interest has been focused on the nanoscale electrode materials to improve the electrochemical performance.[12,13] Especially, the one-dimensional (1D) nanostructured materials have attracted great interest in their development of the next generation of lithium-ion batteries, because of their high surface-to-volume ratio and excellent electronic transport property.[14−16] Therefore, $ZnCo_2O_4$ 1D nanostructures are expected to show superior capacity and cycling performance. $ZnCo_2O_4$ 1D nanostructures have not been obtained up to now, because of its spinel structure; however, some other 1D nanostructures with the spinel structure have been achieved.[17−19]

Herein, we report the synthesis of porous $ZnCo_2O_4$ nanowires via annealing of a sacrifice template ($ZnCo_2(C_2O_4)_3$ nanowires). The diameters and lengths of $ZnCo_2O_4$ nanowires can be tuned by $ZnCo_2(C_2O_4)_3$ nanowires. The porosity and surface area of $ZnCo_2O_4$ nanowires can be controlled by the annealing temperature. The as-synthesized porous $ZnCo_2O_4$ nanowires were applied as anode materials of Li-ion battery, which showed superior capacity and cycling performance. The effects of the porosity and surface area on the superior capacity and cycling performance also have been discussed.

EXPERIMENTAL SECTION

One gram (1 g) of cetyltrimethylammonium bromide (CTAB) was dissolved in a mixture of 35 mL of cyclohexane and 1.5 mL of *n*-pentanol, which was stirred for 30 min to form a microemulsion. Then, 2 mL of 1 M $H_2C_2O_4$ aqueous solution was added into the above solution and the mixture was stirred for an additional 1 h. Finally, 1.25 mL of an aqueous solution containing 0.05 M $Zn(NO_3)_2$ and 0.1 M $Co(NO_3)_2$ was added to the above-mentioned microemulsion and stirred for 2 h at room temperature. The precipitates (pink) were obtained by centrifugation and dried in air at 80 °C. The precipitates were heated at 500−700 °C for 3 h to obtain the final product (dark gray).

The obtained samples were characterized via powder X-ray diffraction (XRD), using a Rigaku D/max-ga X-ray diffractometer with graphite monochromatized Cu Kα radiation (γ = 1.54178 Å). The morphology and structure of the samples were examined by field-emission scanning electron microscopy (FESEM, Hitachi Model S-4800), transmission electron microscopy (TEM, JEOL Model JEM-200 CX, 160 kV), and high-resolution transmission electron microscopy (HRTEM, JEOL Model JEM-2010) with an energy-dispersive X-ray spectrometer (EDX). The infrared (IR) spectra were measured with a Nicolet Nexus FTIR 670 spectrophotometer. The Brunauer−Emmett−Teller (BET)

Received: October 22, 2010
Published: March 11, 2011

ACS Publications © 2011 American Chemical Society

dx.doi.org/10.1021/ic102129w | *Inorg. Chem.* 2011, 50, 3320–3324

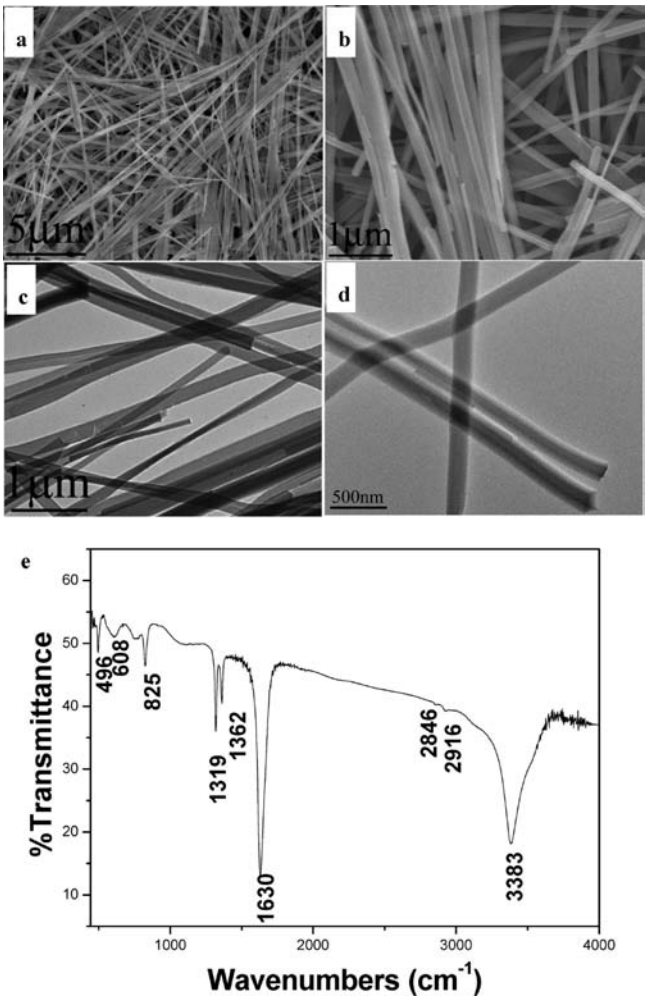

Figure 1. Morphological and structural characterizations of as-synthesized $ZnCo_2(C_2O_4)_3$ nanowires: (a, b) SEM images; (c, d) TEM images; and (e) FTIR spectrum.

surface area and pore volume were tested using a Beckman Coulter Omnisorp100cx system.

Electrochemical measurements were carried out using two-electrode cells with lithium metal as the counter and reference electrodes. The working electrodes of the active material (porous $ZnCo_2O_4$ nanowires), conductive material (acetylene black, ATB), and binder (polytetrafluoroethylene, PTFE) in a weight ratio of $ZnCo_2O_4$/ATB/PTFE = 8:1:1. The electrode was dried at 80 °C for 1 h and cut into a disk (1.0 cm^{-2}). The electrolyte solution was 1 M $LiPF_6$ dissolved in a mixture of ethylene carbonate (EC), propylene carbonate (PC), and diethyl carbonate (DEC) with the volume ratio of EC/PC/DEC = 3:1:1. The cell assembly was performed in a glovebox filled with pure argon (99.999%) in the presence of an oxygen scavenger and a sodium-drying agent. The electrode capacity was measured by a galvanostatic discharge−charge method at a current density of 100 mA g^{-1} and 20 °C. Charge−discharge cycles were tested with a current density of 100 mA g^{-1} in the potential range of 0.01−3 V. The current−voltage curves were tested at a scan rate of 0.5 mV s^{-1}.

RESULTS AND DISCUSSION

A microemulsion-based method has been developed to synthesize 1D nanostructured materials with well-controlled dimensions.[20−24] Herein, we employ the similar method to synthesize $ZnCo_2(C_2O_4)_3$ nanowires that can act as a sacrifice

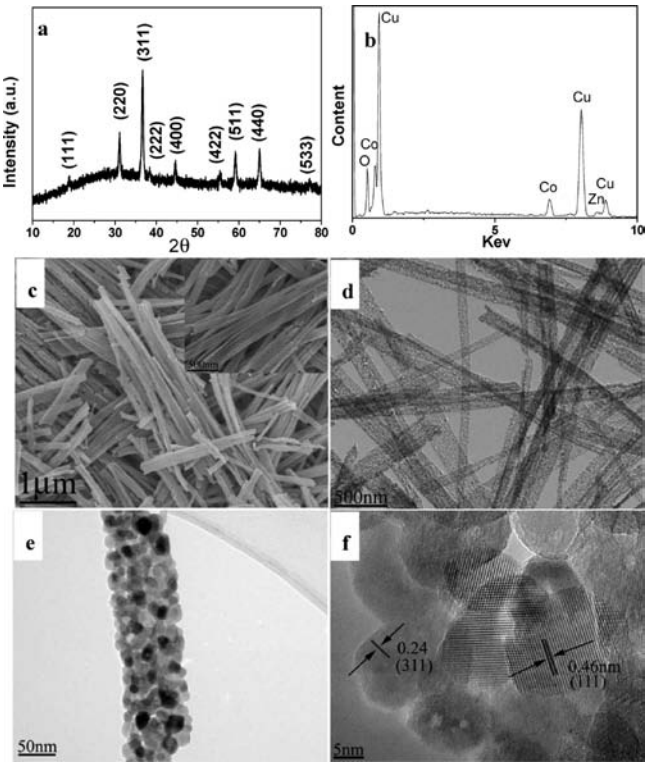

Figure 2. Morphological and structural characterizations of $ZnCo_2O_4$ nanowires synthesized at 500 °C: (a) XRD pattern; (b, c) SEM images; (d, e) TEM images; and (f) HRTEM image.

template for $ZnCo_2O_4$ nanowires. Figures 1a and 1b show the SEM images of as-synthesized products. It can be seen that the as-synthesized products exhibit the morphology of 1D nanowires with diameters of 100−300 nm and lengths on the order of tens of micrometers. The surface of the nanowires is smooth and no isolated nanoparticles can be detected, indicating the synthesis of pure nanowires (see Figures 1c and 1d). The FTIR spectrum was employed to further confirm the composition and surface functional groups of the nanowires (see Figure 1e). The band at 1630, 1362, and 1319 cm^{-1} are assigned to C−O, indicating the presence of bridging oxalates with all four oxygen atoms coordinated to the metal atoms.[25] The O−C−O band appears at 825 cm^{-1}, while other bands located between 450 and 700 cm^{-1} can be assigned to Co−O and Zn−O.[25,26] The relatively weak bands at 2916 and 2846 cm^{-1} are ascribed to the corresponding vibration C−H mode, indicating the existence of residual CTAB as a surfactant. The broad band at 3383 cm^{-1} can be attributed to the water of hydration. The FTIR spectrum indicates the existence of CTAB, which may act as a surfactant to direct the synthesis of $ZnCo_2(C_2O_4)_3$ nanowires.

Figure 2a shows the XRD pattern of the product prepared by the calcination of the amorphous $ZnCo_2(C_2O_4)_3$ nanowires at 500 °C. All diffraction peaks can be indexed as a cubic phase of $ZnCo_2O_4$ with the lattice constant of a = 0.8083 nm, which agrees well with the standard values (JCPDS File Card No. 42-1467). No peaks from other phases are detected. The average diameters of the $ZnCo_2O_4$ nanoparticles calculated from the XRD pattern is ~13 nm, according to the Scherrer formula. It can be seen from the EDX pattern (Figure 2b) that Co, Zn, and O may come from $ZnCo_2O_4$, while Cu should originate from the substrate. Moreover, the molar ratio of Zn to Co can be

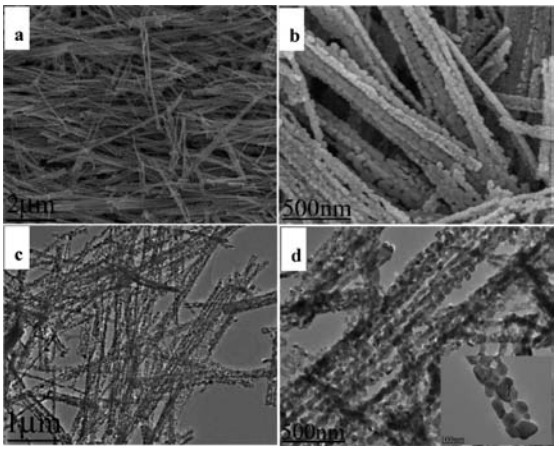

Figure 3. Morphological characterizations of $ZnCo_2O_4$ nanowires synthesized at 700 °C: (a, b) SEM images; (c, d) TEM images.

calculated to be 2.45:4.88, which is basically consistent with the XRD pattern. We believe that the XRD pattern, combined with the EDX pattern, can confirm the synthesis of $ZnCo_2O_4$. Figure 2c and the inset image show the SEM images of as-synthesized $ZnCo_2O_4$. It can be seen that the as-synthesized $ZnCo_2O_4$ maintains the morphology of 1D nanowires with diameters of 100−300 nm and lengths of several micrometers. It is obvious that the nanowires have been cut down and the surface of the $ZnCo_2O_4$ nanowires becomes rough, compared to that of $ZnCo_2(C_2O_4)_3$ nanowires, because of the release of CO_2 and the crystallization and grain growth under the high annealing temperature. The TEM image (Figure 2d) shows that no isolated nanoparticles can be detected, indicating the synthesis of $ZnCo_2O_4$ nanowires. Figure 2e shows the TEM image of an individual $ZnCo_2O_4$ nanowire. It can be seen that the nanowire consists of $ZnCo_2O_4$ nanocrystals with diameters of 5−20 nm, which arrange linearly and connect with each other to form a stable nanowire. Many pores with diameters of ~5 nm can be detected between $ZnCo_2O_4$ nanocrystals, because of the decomposition of $ZnCo_2(C_2O_4)_3$ to $ZnCo_2O_4$, which may greatly enhance the surface-to-volume ratio of the nanowires. The HRTEM image (Figure 2f) of an individual $ZnCo_2O_4$ nanowire indicates that there are two types of lattice fringes with lattice spacings of 0.24 and 0.46 nm, corresponding to the {311} and {111} plane of $ZnCo_2O_4$. The above-mentioned characterizations confirm the synthesis of porous $ZnCo_2O_4$ nanowires via annealing of $ZnCo_2(C_2O_4)_3$ nanowires. Figures 3a and 3b show the SEM image of $ZnCo_2O_4$ nanowires synthesized via annealing of $ZnCo_2(C_2O_4)_3$ nanowires at 700 °C. It can be seen that the diameters of the nanocrystals of the as-synthesized $ZnCo_2O_4$ nanowires grow larger, because of the fusion between the nanocrystals at high annealing temperature (700 °C). As observed from the TEM images (see Figures 3c and 3d), the diameters of the composed nanocrystals, along with the nanopores, increase to 30−50 nm, which is consistent with SEM images. Therefore, the morphology of $ZnCo_2O_4$ nanowires can be tuned by the annealing temperature.

The specific surface areas of $ZnCo_2O_4$ nanowires synthesized at different annealing temperature were characterized by Brunauer−Emmett−Teller (BET) analysis using nitrogen adsorption, as shown in Figure 4. It can be seen that the specific surface areas of $ZnCo_2O_4$ nanowires (500 °C) and $ZnCo_2O_4$ nanowires

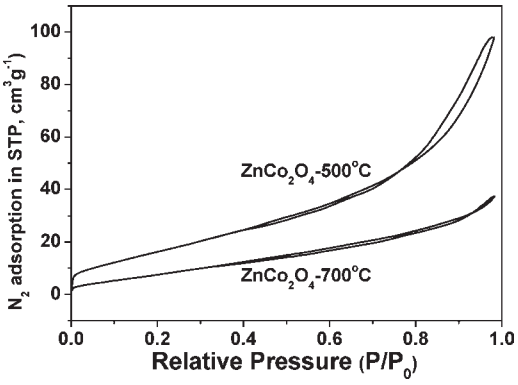

Figure 4. N_2 adsorption/desorption isotherms for $ZnCo_2O_4$ nanowires synthesized at 500 and 700 °C.

(700 °C) are ~68.86 $m^2\ g^{-1}$ and ~35.99 $m^2\ g^{-1}$, respectively, indicating that the surface area of $ZnCo_2O_4$ nanowires decreases as the annealing temperature increases. The enhanced surface area of $ZnCo_2O_4$ nanowires (500 °C) can be attributed to smaller diameters and larger quantities of the nanocrystals and nanopores.

The as-synthesized $ZnCo_2O_4$ nanowires exhibit the porous 1D nanostructures and large surface area and, therefore, can be applied as high-performance anode materials of an Li-ion battery. According to the previous papers,[10,11] the entire electrochemical process can be clarified as follows:

$$ZnCo_2O_4 + 8Li^2 + 8e^- \rightarrow Zn + 2Co + 4Li_2O \quad (1)$$

$$Zn + Li^+ + e^- \leftrightarrow LiZn \quad (2)$$

$$Zn + Li_2O \leftrightarrow ZnO + 2Li^+ + 2e^- \quad (3)$$

$$2Co + 2Li_2O \leftrightarrow 2CoO + 4Li^+ + 4e^- \quad (4)$$

$$2CoO + \frac{2}{3}Li_2O \leftrightarrow \frac{2}{3}Co_3O_4 + \frac{4}{3}Li^+ + \frac{4}{3}e^- \quad (5)$$

When the $ZnCo_2O_4$ nanowires are electrochemically discharged with lithium metal, crystal structure destruction occurs, followed by the formation of nanosized Zn and Co, and Li_2O, as eq 1 shows. Then, the consequent electrochemical process may be the combined reaction, based on the ZnO (eqs 2 and 3) and Co_3O_4 (eqs 3 and 4), respectively. Individual ZnO and Co_3O_4 components, as the anode materials of Li-ion batteries, have been detailed clearly in many papers.

Figure 5a shows the first three cyclic voltammogram (CV) curves of the electrodes made from $ZnCo_2O_4$ nanowires at a scan rate of 0.5 mV s^{-1} and room temperature. The first discharge for the $ZnCo_2O_4$ nanowires shows an irreversible reduction peak with a maximum at 0.75 V, because of the decomposition of $ZnCo_2O_4$ to Zn and Co, which is similar to the previous reports.[11] Compared to the first cycle, the discharge of the second and third cycles shows a peak at 1.1 V, indicative of different electrochemical reactions governing the two processes. However, in the anodic polarization process, two peaks are recorded, at ~1.7 V and ~2.3 V, which can be attributed to the oxidation of Zn^0 to Zn^{2+} and Co^0 to Co^{3+}. Figure 5b shows the 1st, 10th, and 20th discharge curves of the electrodes made from the $ZnCo_2O_4$ nanowires at a current rate of 100 mA h/g

dx.doi.org/10.1021/ic102129w |Inorg. Chem. 2011, 50, 3320–3324

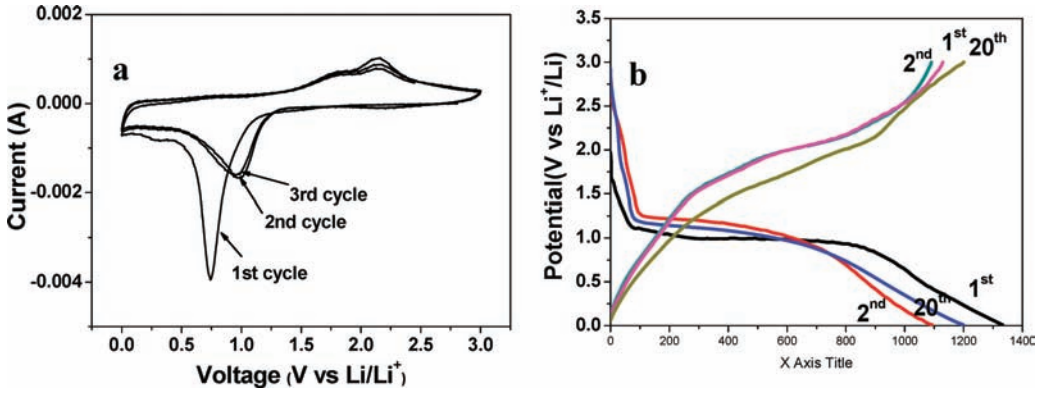

Figure 5. The first three cyclic voltammogram (CV) curves of the electrodes made from $ZnCo_2O_4$ nanowires at a scan rate of 0.5 mV s^{-1} and room temperature.

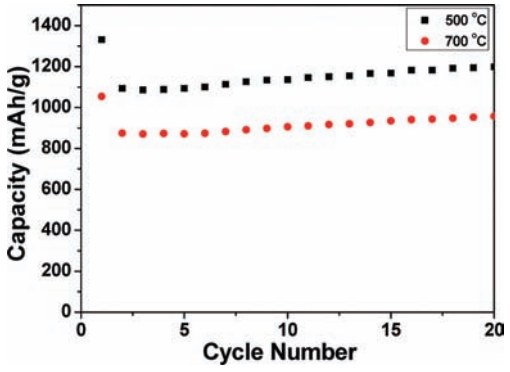

Figure 6. Discharge capacity versus cycle number for the electrodes made from the porous $ZnCo_2O_4$ nanowires synthesized at 500 and 700 °C.

and in the voltage window of 0.005−3 V. It can be seen that all three discharge curves exhibit one plateau between 0.7 V and 1.2 V, while the plateau of the second and third discharge curves is slightly higher than that of the first discharge curves, which is similar to the previous reports.[11] The discharge capacities of the electrode in the 1st, 10th, and 20th cycles are 1331.5, 1092.9, and 1197.9 mA h/g, respectively. The reversible capacity of the $ZnCo_2O_4$ nanowires is much higher than that of $ZnCo_2O_4$ nanoparticles.[10,11] The large surface area and unique porous 1D nanostructures may be responsible for the high capacity. However, the initial Coulombic efficiency for the porous $ZnCo_2O_4$ nanowires is ∼82%, which can be ascribed to the formation of the solid electrolyte interface (SEI) film and some undecomposed Li_2O phase. Figure 6 shows the discharge capacity versus the number of cycles for the electrodes made from the porous $ZnCo_2O_4$ nanowires synthesized at 500 and 700 °C, respectively. It can be seen that the reversible capacity of $ZnCo_2O_4$ nanowires synthesized at 500 °C is maintained at ∼1197 mA h/g after 20 cycles, while the $ZnCo_2O_4$ nanowires synthesized at 700 °C exhibit a value of ∼957 mA h/g. The fact that the surface area of the $ZnCo_2O_4$ nanowires synthesized at 500 °C (68.86 m^2 g^{-1}) is larger than that of the $ZnCo_2O_4$ nanowires synthesized at 700 °C (35.99 m^2 g^{-1}) may explain this phenomenon. It can be concluded that the as-synthesized porous $ZnCo_2O_4$ nanowires exhibit large capacity and good cyclic performance as anode materials of Li-ion battery. The large surface area and unique porous 1D nanostructures may be responsible for the good performance. In order to further explain the electrochemical processes, the materials after 20 cycles have been characterized by SEM, TEM, SAED, and XRD analysis. Figure 7a show the XRD pattern of the porous $ZnCo_2O_4$ nanowires after 20-cycle charge−discharge processes. It can be seen that the Cu peaks originated from the substrate are strong while the other peaks are faint. This can be explained by that the oxidized-electrode constituents are nanosized and the spinel structure is mostly destroyed during the charge−discharge processes.[11] However, three weak peaks between 30° and 40° can be basically attributed to ZnO and Co_3O_4, indicating that ZnO and Co_3O_4 act as anode materials, instead of $ZnCo_2O_4$, in the following charge−discharge preocesses. As mentioned above, ZnO and Co_3O_4 can benefit from each other as a matrix to buffer the volume change. It is also important to explore the morphology of the resultant materials after 20 cycles, which can indicate the merit of the porous nanowire structure during the charge−discharge processes. Figures 7b and 7c show the SEM and TEM images of the resultant materials after 20 cycles. It can be seen that the porous nanowire structure are basically maintained. However, the porous nanowires have been cut down and seem contorted, because of the large volume change during the charge−discharge processes. Compared to the nanoparticles, the porous nanowires have the 1D nanostructure and many nanopores and, thus, can effectively buffer the volume changes. Figure 7d shows the SAED pattern of the resultant materials. The *d*-spacing calculated from some points may correspond to the ZnO and Co_3O_4, which is consistent with the XRD pattern, and further confirms that the resultant materials are composed of ZnO and Co_3O_4. The above discussions also confirm the entire electrochemical process of $ZnCo_2O_4$ as the anode materials in Li-ion batteries.

CONCLUSION

We have synthesized porous $ZnCo_2O_4$ nanowires via annealing of $ZnCo_2(C_2O_4)_3$ nanowires as sacrificial templates. The morphology and surface area of as-synthesized porous $ZnCo_2O_4$ nanowires can be tuned using the annealing temperature. The porous $ZnCo_2O_4$ nanowires synthesized at 500 °C exhibit small diameters and large surface area than that synthesized at 700 °C. The as-synthesized porous $ZnCo_2O_4$ nanowires have been applied as the anode of Li-ion batteries, which show superior capacity and cycling performance. The porous 1D nanostructures and large surface area are responsible for the superior performance. Moreover, the porous $ZnCo_2O_4$ nanowires

dx.doi.org/10.1021/ic102129w |*Inorg. Chem.* 2011, 50, 3320–3324

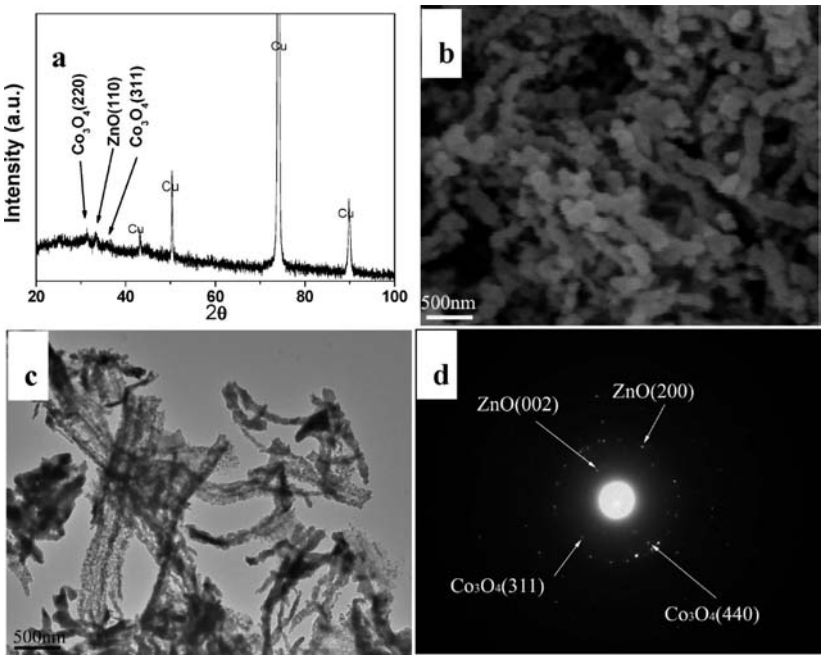

Figure 7. Morphological and structural characterizations of the resultant materials after 20 cycles: (a) XRD pattern; (b) SEM image; (c) TEM image; (d) SAED pattern.

synthesized at 500 °C show larger capacity and better cycling performance than that prepared at 700 °C, because of their higher porosity and larger surface area.

AUTHOR INFORMATION

Corresponding Author

*Tel.: 86-571-87951667. Fax: 86-571-87952322. E-mail: mseyang@zju.edu.cn.

ACKNOWLEDGMENT

The authors would like to appreciate the financial support from 973 Project (No. 2007CB613403), 863 Project (No. 2007AA02Z476), NSFC (No. 51002133), and a China Postdoctoral Science Foundation-funded project (No. 20090461350).

REFERENCES

(1) Poizot, P.; Laruelle, S.; Grugeon, S.; Dupont, L.; Tarascon, J. M. *Nature* **2000**, *407*, 496.
(2) Li, W. Y.; Xu, L. N.; Chen, J. *Adv. Funct. Mater.* **2005**, *15*, 851.
(3) Yu, Y.; Chen, C. H.; Shui, J. L.; Xie, S. *Angew. Chem., Int. Ed.* **2005**, *44*, 2.
(4) Nam, K. T.; Kim, D. W.; Yoo, P. J.; Chiang, C. Y.; Meethong, N. L.; Hammond, P .T.; Chiang, Y. M.; Belcher, A. M. *Science* **2006**, *312*, 885.
(5) Du, N.; Zhang, H.; Chen, B. D.; Wu, J. B.; Ma, X. Y.; Liu, Z. H.; Zhang, Y. Q.; Yang, D. R.; Huang, X. H.; Tu, J. P. *Adv. Mater.* **2007**, *19*, 4505.
(6) Kang, Y. M.; Kim, K. T.; Kim, J. H.; Kim, H. S.; Lee, P. S.; Lee, J. Y.; Liu, H. K.; Dou, S. X. *J. Power Sources* **2004**, *133*, 252.
(7) Chu, Y. Q.; Fu, Z. W.; Qin, Q. Z. *Electrochim. Acta* **2004**, *49*, 4815.
(8) Sharama, Y.; Sharama, N.; Rao, G. V. S.; Chowdari, B. V. R. *J. Power Sources* **2009**, *173*, 495.
(9) Wang, G.; Gao, X. P.; Shen, P. W. *J. Power Sources* **2009**, *192*, 719.
(10) Ai, C. C.; Yin, M. C.; Wang, C. W.; Sun, J. T. *J. Mater. Sci.* **2004**, *39*, 1077.
(11) Shamara, Y.; Shamara, N.; Rao, G. V. S.; Chowdari, B. V. R. *Adv. Funct. Mater.* **2007**, *17*, 2855.
(12) Singhal, A.; Skandan, G.; Amatucci, G.; Badway, F.; Ye, N.; Manthiram, A.; Ye, H.; Xu, J. J. *J. Power Sources* **2004**, *129*, 38.
(13) Arico, A. S.; Bruce, P.; Scrosati, B.; Tarascon, J. M.; Schalkwijk, W. V. *Nat. Mater.* **2005**, *4*, 366.
(14) Chen, J.; Tao, Z. L.; Li, S. L. *Angew. Chem., Int. Ed.* **2003**, *42*, 2147.
(15) Wang, Y.; Lee, J. Y.; Zeng, H. C. *Chem. Mater.* **2005**, *17*, 3889.
(16) Chan, C. K.; Peng, H. L.; Liu, G.; Mcilwrath, K.; Zhang, X. F.; Huggins, R. A.; Cui, Y. *Nature Nanotechnol.* **2008**, *3*, 31.
(17) Wu, X. C.; Tao, Y. R.; Han, Z. J.; Zhang, B. D. *J. Mater. Chem.* **2003**, *13*, 2649.
(18) Fan, H. J.; Knez, M.; Scholz, R.; Nielsch, K.; Pippel, E.; Hesse, D.; Zacharias, M.; Gösele, U. *Nat. Mater.* **2006**, *5*, 627.
(19) Lee, H.-W.; Muralidharan, P.; Ruffo, R.; Mari, C. M.; Cui, Y.; Kim, D. K. *Nano Lett.* **2010**, *10*, 3852.
(20) Trentler, T. J.; Hickman, K. M.; Goel, S. C.; Viano, A. M.; Gibbons, P. C.; Murphy, C. J. *Science* **1995**, *270*, 1791.
(21) Murphy, C. J. *Science* **2002**, *298*, 2139.
(22) Cao, M.; Hu, C.; Wang, E. *J. Am. Chem. Soc.* **2003**, *125*, 11196.
(23) Hirai, T.; Kobayashi, J.; Komasawa, I. *Langmuir* **1999**, *15*, 6291.
(24) Zhang, Z .T.; Rondinone, A. J.; Ma, J. X.; Shen, J.; Dai, S. *Adv. Mater.* **2005**, *17*, 1415.
(25) Ren, L.; Wang, P. P.; Han, Y. S.; Hu, C. W.; Wei, B. Q. *Chem. Phys. Lett.* **2009**, *476*, 78.
(26) Wei, X. H.; Chen, D. H.; Tang, W. J. *Mater. Chem. Phys.* **2007**, *103*, 54.